optica

Gouy phase shift of a tightly focused, radially polarized beam

Korbinian J. Kaltenecker,[1,2,3,*] Jacob C. König-Otto,[4,5] Martin Mittendorff,[4,6] Stephan Winnerl,[4] Harald Schneider,[4] Manfred Helm,[4,5] Hanspeter Helm,[2,3] Markus Walther,[2,3] and Bernd M. Fischer[1]

[1]French-German Research Institute of Saint-Louis, 5, Rue du Général Cassagnou 68301, Saint-Louis, France
[2]Institute of Physics, University of Freiburg, Hermann-Herder-Strasse 3, 79104 Freiburg, Germany
[3]Freiburg Materials Research Center, University of Freiburg, Stefan-Meier-Strasse 21, 79104 Freiburg, Germany
[4]Institute of Ion Beam Physics and Materials Research, Helmholtz-Zentrum Dresden Rossendorf, P.O. Box 510119, 01314 Dresden, Germany
[5]Institute of Applied Physics, TU Dresden, 01062 Dresden, Germany
[6]Institute for Research in Electronics and Applied Physics, University of Maryland, College Park, Maryland 20742, USA
*Corresponding author: Korbinian.Kaltenecker@physik.uni-freiburg.de

Received 23 July 2015; revised 4 November 2015; accepted 24 November 2015 (Doc. ID 246573); published 7 January 2016

Radially polarized beams represent an important member of the family of vector beams, in particular due to the possibility of using them to create strong and tightly focused longitudinal fields, a fundamental property that has been exploited by applications ranging from microscopy to particle acceleration. Since the properties of such a focused beam are intimately related to the Gouy phase shift, proper knowledge of its behavior is crucial. Terahertz microscopic imaging is used to extract the Gouy phase shift of the transverse and longitudinal field components of a tightly focused, radially polarized beam. Since the applied terahertz time-domain approach is capable of mapping the amplitude and phase of an electromagnetic wave in space, we are able to directly trace the evolution of the geometric phase as the wave propagates through the focus. We observe a Gouy phase shift of 2π for the transverse and of π for the longitudinal component. Our experimental procedure is universal and may be applied to determine the geometric phase of other vector beams, such as optical vortices, or even arbitrarily shaped and polarized propagating waves.

OCIS codes: (110.6795) Terahertz imaging; (110.7348) Wavefront encoding; (120.5050) Phase measurement; (260.5430) Polarization.

http://dx.doi.org/10.1364/OPTICA.3.000035

1. INTRODUCTION

The Gouy phase is a well-known phenomenon in optics. It describes the effect in which an electromagnetic beam propagating through a focus experiences an additional phase shift with respect to a plane wave. This phase anomaly was first described by Gouy in 1890 [1], and since then, its physical origin and its consequences have been extensively investigated theoretically as well as experimentally. The Gouy phase shift is a fundamental physical property of any kind of wave that is subjected to transverse spatial confinement, for example, due to focusing or diffraction on small apertures. An intuitive description can be given based on the geometrical properties of Gaussian beams [2]. More sophisticated theories describe the Gouy phase shift as a geometrical quantum effect due to Heisenberg's uncertainty relations [3,4], or as a manifestation of Berry's geometrical phase [5–7]. The Gouy phase has important consequences in optics. It determines the resonant frequencies in laser cavities [8], is crucial for the generation of ultra-short laser pulses [9,10] and the formation of optical bottle beams [11], and affects the propagation dynamics of optical vortices [12]. The Gouy phase shift finds applications in achieving transverse and axial super-resolutions in the optical regime [13], as well as sub-wavelength spatial resolution in terahertz imaging [14]. Apart from electromagnetic waves, the Gouy phase shift has also been observed in matter waves [15,16], surface plasmon polaritons [17], phonon polaritons [18], and acoustic pulses [19,20].

Most measurements of the optical Gouy phase have been performed in the spatial domain using two-beam interferometry [1,21,22]. The phase was also observed by the spatial mode interference-locking method [23], the stereo-above-threshold-ionization scheme to measure the carrier-envelope phase [9], or by using wavefront sensors [24]. Due to its unique capability to simultaneously access the amplitude and phase of an electromagnetic wave, terahertz time-domain sensing and imaging technology provides a unique possibility to investigate the Gouy phase [25]. As prominent examples, the polarity reversal of focused terahertz pulses due to the Gouy phase shift was directly measured [26], as well as the Gouy phase shift of scattered terahertz pulses from cylindrical or spherical targets [27]. A complete spatial characterization of the Gouy phase shift by terahertz digital holography was presented in [28].

Here, we experimentally investigate the Gouy phase shift of tightly focused, radially polarized terahertz transients. Radially

polarized light is a special type of Bessel–Gauss beam, the so called cylindrical vector beam [29,30], where the electric field vector is pointing in the plane of the beam cross section to the radial direction. The light from such polarization exhibits pronounced longitudinal fields that feature a smaller beam waist in the focus as compared to the transverse fields of a linearly polarized Gaussian beam [31–33]. The unique vectorial field distribution of radially polarized vector beams in the focus has apparent applications in high-resolution imaging and microscopy [30]. Furthermore, the transverse fields of such beams are also applied in microscopy, namely in stimulated emission depletion microscopy [34].

In case of weakly focused beams, the transverse electric field component of radially polarized light can be described within the paraxial approximation yielding

$$\boldsymbol{E}_{\mathrm{rad}}(\rho,z,t) = E_0 \frac{w_0}{w^2(z)}\hat{\boldsymbol{\rho}} l_0(\rho,z) \cdot \exp\left[i\left(kz - 2\arctan\frac{z}{z_0}\right)\right]\exp[-i\omega t], \quad (1)$$

where $\rho = (x^2+y^2)^{1/2}$ and $\hat{\boldsymbol{\rho}} = (x,y,0)/\rho$ are unit vectors pointing in the radial direction. The radial amplitude function $l_0(\rho,z)$ is given by:

$$l_0(\rho,z) = \rho \exp\left[ik\frac{\rho^2}{2R(z)}\right]\exp\left[-\frac{\rho^2}{w^2(z)}\right]. \quad (2)$$

The exact expressions for the Rayleigh range z_0, the beam waist $w(z)$, and the radius of curvature $R(z)$ are given in the Supplement 1. Equation (1) contains the analytical expression

$$\phi_{\mathrm{Gouy}}(z) = 2\arctan\frac{z}{z_0}, \quad (3)$$

which corresponds to a total Gouy phase shift of 2π for radially polarized light in the paraxial approximation. However, in reality, the phase behavior of focused, radially polarized beams turns out to be more complicated. This was indicated by the observation that their wavefront spacing near the focus is highly irregular [35]. In a subsequent theoretical study, the Gouy phase shift of the longitudinal component of the electric field vector at the focal plane was investigated, and it was predicted that this vector component experiences a Gouy phase shift by π [36]. On the other hand, the radial component should yield, as expected, a phase shift by 2π [37]. Note that the analytical expression in Eq. (3) can only be derived within the paraxial approximation. For tightly focused beams beyond the paraxial approximation, the Gouy phase shifts of the transverse components can be determined by numerical simulations. Furthermore, the paraxial approximation cannot yield an expression for the longitudinal fields, since the approximation affects terms that are vital for determining the longitudinal field. Very recently, electron acceleration by longitudinal terahertz fields generated by focusing radially polarized beams has been demonstrated [38]. This promising approach for realizing compact particle accelerators requires detailed knowledge of the Gouy phase shift, as the phase and group velocities are of crucial importance for the acceleration process.

Radially polarized light has been generated in the visible or infrared frequency regimes using special polarization conversion optics [39–41]. In the terahertz regime, radially polarized terahertz pulses have been produced either via velocity-mismatched optical rectification in (001)-oriented ZnTe [42], or by photoconductive emitters consisting of single-ring electrodes. The latter emitters have been used, for example, to achieve enhanced coupling to the plasmonic surface modes of metal wires [43–45], or for optimal plasmonic focusing on a metal disc [46]. The intensity of radially polarized pulses can be significantly enhanced using large-area emitters consisting of multiple interdigitated ring electrodes that are alternately shielded from the excitation beam [47]. In this paper, we use the latter type of emitter for the generation of radially polarized terahertz pulses in order to experimentally investigate the Gouy phase shift of focused, radially polarized light.

2. EXPERIMENTAL DETAILS

Our approach is based on mapping the electric field components of a focused terahertz beam in a plane defined by the propagation direction along the z-axis and a radial direction ρ, with the focal point in the center of the two-dimensional map. For this purpose, we use a terahertz near-field microscope, which is capable of mapping the field distribution with a spatial resolution well below the diffraction limit [48,49]. Such a system has been used to investigate the near fields of sub-wavelength-sized structures [48,50], and also to study wave propagation along surfaces or in free space [51,52].

Figure 1 illustrates the near-field microscope, which relies on the terahertz time-domain spectroscopy approach. A femtosecond laser beam is divided by a beam splitter into two beams, gating the emitter antenna and the detector crystal. The antenna layout of the photoconductive emitter is shown in Fig. 2(a). It possesses a radially symmetric, interdigitated finger electrode structure [47] biased with 15 V. Due to the change of the bias field direction for neighboring electrode gaps, which would result in destructive interference of the emitted terahertz wavelets in the far field, every second gap is shielded by a metallic cover, as indicated in Fig. 2(a). The laser excitation beam illuminates a 300 μm-diameter spot centered on the emitter structure. The emitted radially polarized terahertz pulse is collimated and refocused by two off-axis paraboloidal mirrors with a focal length of $f = 100$ mm. In order to collect the divergent radiation of the emitter, the mirrors are designed with a very large entrance aperture angle of 60° corresponding to a NA = 0.87. This mirror optics generates a diffraction-limited, one-to-one image of the source. The optical pulse is focused through a 1 mm-thick ZnTe crystal, but is reflected by a

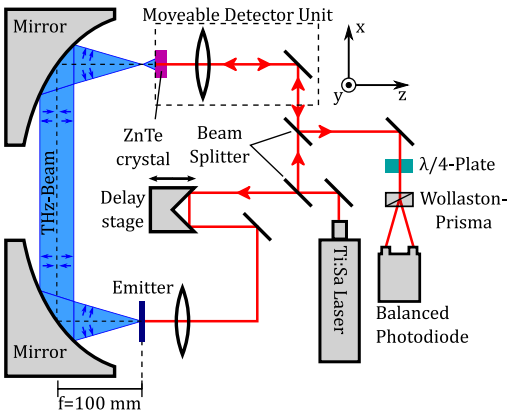

Fig. 1. Schematic illustration of the terahertz near-field microscope.

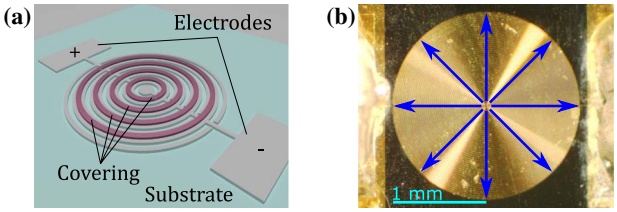

Fig. 2. (a) Sketch of the radial emitter and (b) photograph of the radial emitter. The blue arrows indicate the polarization of the emitted field.

highly reflective coating on the object side. The back-reflected laser beam experiences polarization rotation by the local terahertz electric field. The degree of rotation is measured by balanced photo-detection. By using ZnTe-crystals cut along different crystal axes, the transverse and longitudinal components (E_ρ and E_z) of the electric field can be measured separately [53,54]. By raster scanning the electro-optic crystal together with the laser, the electric field profile of the terahertz beam can be spatially mapped.

We performed scans of 4 mm in the radial and 6 mm in the propagation directions, with a spatial resolution of 40 μm. Note that at each position, the entire time-domain signal of the terahertz field is recorded with a temporal resolution of 67 fs, thus yielding a spatial field distribution at each time step.

A temporal snapshot of the measured radial component of the electric field E_ρ is shown in Fig. 3(a) for a radially polarized terahertz pulse at the instant that it passes through its focus. The corresponding field transients measured at the positions of the highest field amplitudes are shown in Fig. 3(b). The recorded pulses at the two positions have opposite polarity with a temporal evolution that is inverted, as is expected for a radially polarized beam. A Fourier transformation yields the complex amplitude in the frequency domain. In Fig. 3(c), we plot the real part of the electric field E_ρ at one particular frequency ($\nu = 1.35$ THz). In this plot, the individual wavefronts of the radially anti-symmetrical field become visible. Note that slight asymmetries in all measurements are caused by misalignment and are due to laser drifts during a spatial scan (top to bottom of the image), which takes several hours. The corresponding spectra of the two sample pulses in Fig. 3(b) are shown in Fig. 3(d) as the real part of the electric field in the frequency domain, demonstrating anti-symmetry at all frequencies between 0.5 and 2.5 THz.

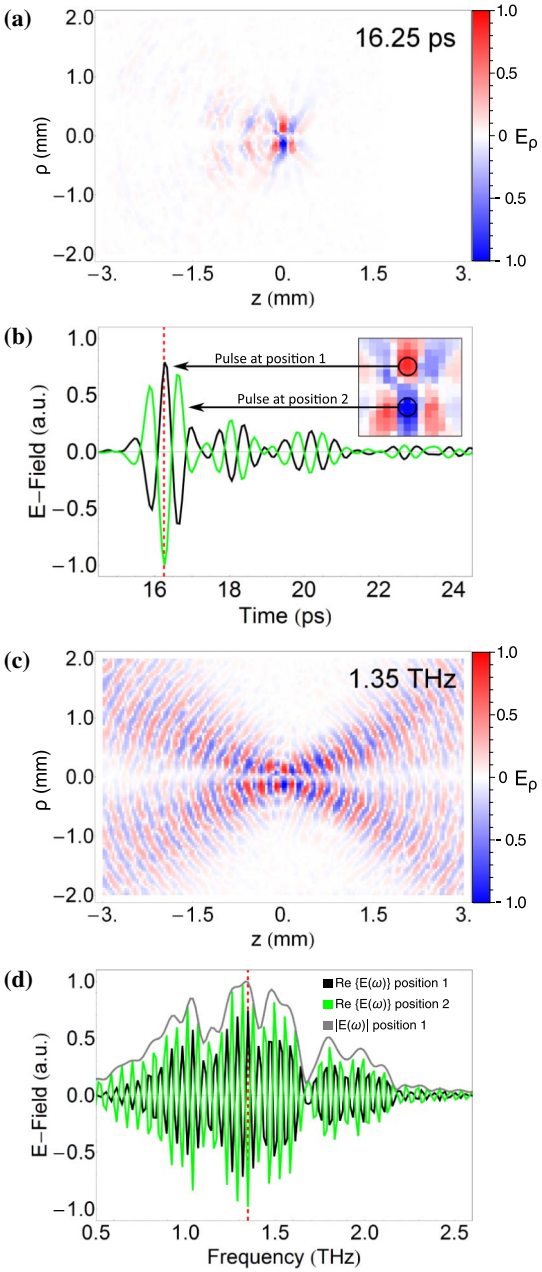

Fig. 3. (a) Measured field map of a radially polarized terahertz pulse plotted as it passes through the focus. Color code has been normalized to the maximum field strengths. (b) Corresponding field transients at the position of highest field amplitudes. (c) Real part of the electric field amplitude plotted at a frequency of 1.35 THz. (d) Frequency dependence of the field amplitude of the pulses in (b).

3. EXTRACTION OF THE GOUY PHASE

In order to extract the Gouy phase shift from the measured data, we follow the intuitive procedure illustrated in Fig. 4. In the first step, at a given frequency, all electric field values associated with a certain wavefront (as indicated by the black semicircles) are integrated along this wavefront in either the lower or the upper half-space of Fig. 4(a) and are assigned to the intersection point of the wavefront with the optical axes (red dots). Note that integration in the two half-spaces yields values of identical magnitude but opposite signs. By this integration the measured two-dimensional field maps are effectively projected onto the optical axis and reduced to only one dimension. For this purpose, we initially need to identify the circular sections, which describe the wavefronts in proximity to the Gaussian focus.

Theoretically, only the three parameters E_0, ω, and w_0 are necessary to characterize the radially polarized beam completely. Since the field amplitude and frequency are fixed for each field map, only w_0 needs to be determined from the experimental data. This is accomplished by fitting to our data the expression for the transverse field profile at the beam focus $z = 0$, reducing Eq. (1) to

$$E(\rho) = E_0|\rho| \exp\left(-\frac{\rho^2}{w_0^2}\right), \tag{4}$$

with E_0 and w_0 as the fitting parameters. With the extracted beam waists, we are able to calculate the wavefront radius of curvature

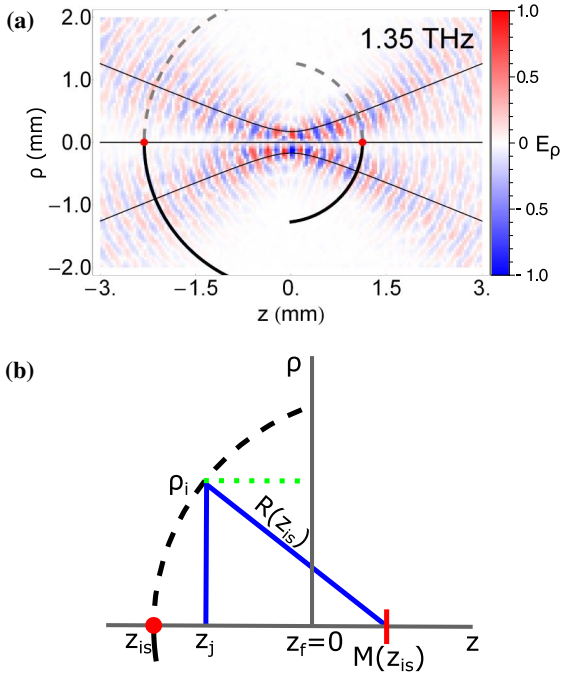

Fig. 4. Illustration of the procedure used to project the two-dimensional field maps onto only one dimension.

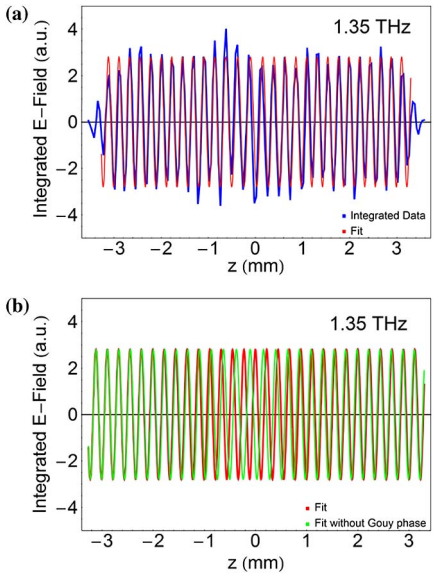

Fig. 5. Transverse component of the radially polarized beam: (a) projected and integrated field data and fit and (b) comparison of fit with and without Gouy phase term.

$R(z_{is})$ (see Supplement 1). Note that z_{is} denotes the intersection of the circle with the optical axis [red dots in Fig. 4(a)]. Also, the center of each circle is located on the optical axis and is given by

$$M(z_{is}) = z_{is} - R(z_{is}) = -\frac{z_0^2}{z_{is}}. \tag{5}$$

As indicated in Fig. 4(a) for two wavefronts, the one before (left) and the one after (right) passing through the focus, i.e., for $z_{is} < 0$ and $z_{is} > 0$, the measured wavefronts nicely follow the calculated semicircles. Now, the field amplitudes along each wavefront need to be summed up. For this purpose, we can calculate for each pixel the intersection point of its wavefront semicircle with the optical axis. From Fig. 4(b), we find that for a spatial pixel (ρ_i, z_j)

$$\rho_i^2 + (z_j - M(z_{is}))^2 = R(z_{is})^2, \tag{6}$$

which reduces to

$$z_{is}^3 - z_{is}(\rho_i^2 + z_j^2 - 2z_0^2) - 2z_j z_0^2 = 0. \tag{7}$$

By solving this equation for z_{is}, we can associate each pixel with a point z_{is} on the optical axis. Note that Eq. (7) in general has three solutions, but the constraints that the solution needs to be real-valued and that the intersection point z_{is} needs to have the same sign as z_j leave only one valid solution. Finally, the optical axis is divided into intervals of 40 μm and all pixels that are associated with z_{is} values within one interval are summed up (integrated data).

4. GOUY PHASE SHIFT FOR TRANSVERSE FIELD COMPONENTS

With the procedure described in the previous section, the integrated field data projected onto the z-axis are obtained [see blue curve in Fig. 5(a)]. In order to extract the Gouy phase shift from the wavefront integrated electric field, we have fitted a general expression of the form

$$E(z) = A \sin\left(\frac{2\pi}{\lambda}z + \zeta + n \arctan\left(\frac{z}{z_0}\right)\right), \tag{8}$$

with A, ζ and n as free-fitting parameters to the data, with $\lambda = c/\nu$ and z_0 being fixed for each particular frequency. The parameter ζ is an arbitrary constant phase required to adjust the initial phase of the fit. The pre-factor n corresponds to the complete Gouy phase shift in multiples of π experienced by the wave upon transversing the focus. The best fit to our data is also plotted in Fig. 5(a) (red curve).

The effect of the Gouy phase is illustrated in Fig. 5(b), where the fitted function [Eq. (8)] with (red curve) and without (green curve) the phase term $n \cdot \arctan z/z_0$ is plotted. Whereas both functions are initially in phase, at the focus ($z = 0$), they have a phase difference of π and after passing the focus, they eventually are in phase again, which corresponds to an overall Gouy phase shift of 2π.

In order to trace the evolution of the phase in space, we follow an alternative procedure based on fitting the suitable wave function only within a narrow spatial window and successively moving the window stepwise along the z-axis (step size 40 μm). Using the expression for a spatially oscillating wave

$$E(z) = A \sin\left(\frac{2\pi}{\lambda}z + \phi_{\text{Gouy}}(z)\right), \tag{9}$$

with A and ϕ_{Gouy} as free-fitting parameters, the accumulated Gouy phase shift can be spatially traced. The spatial dependence of the Gouy phase obtained from the fit is presented in Fig. 6(a) for our central frequency of 1.35 THz (red line). For comparison, we also plot the Gouy phase term of the paraxial approximation $n \cdot \arctan z/z_0$ for $n = 2$ and $z_0 = 393$ μm (dashed line). In Fig. 6(b), we compare the phase shift extracted for different frequencies. The curves become steeper with increasing frequencies, as expected due to the decrease of the Rayleigh length z_0 with

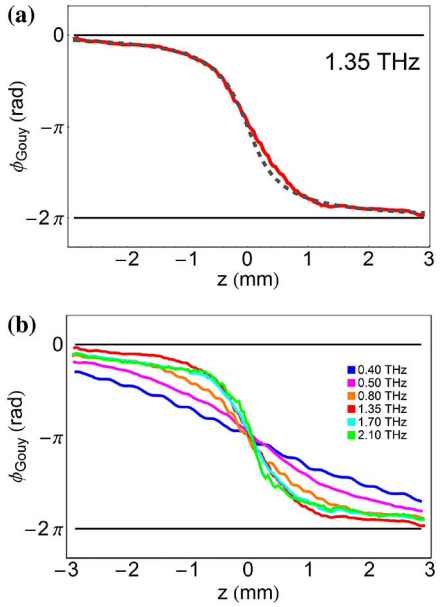

Fig. 6. Transverse component of the radially polarized beam: (a) Gouy phase shift at 1.35 THz and (b) compilation of several other frequencies.

increasing frequency. For the lowest frequencies, 0.4 and 0.5 THz, the phase shift occurs over the entire z-range covered in our scan, while for higher frequencies, the main change occurs within a narrow window close to the focus.

5. GOUY PHASE SHIFT FOR LONGITUDINAL FIELD COMPONENTS

Having characterized the transverse component of the electric field of the radially polarized beam, we next investigate its longitudinal field component. The corresponding electric field map of E_z is shown in Fig. 7 for two selected frequencies. In contrast to the radial component, the longitudinal part only has a strong contribution in the vicinity of the focus, with the strongest field directly in its center. This concentration of the E_z field component is clearly visible in the field maps at higher frequencies, e.g., for 1.35 THz.

For this case, we again plot the field projected onto the optical axis using the described procedure. The measured data together with a fit according to Eq. (8) are shown in Fig. 8(a). In this case, we obtain a total Gouy phase shift of only π, which can be clearly seen in Fig. 8(b), where again, the fitted function is compared with a wave lacking the Gouy phase term. While initially in phase, the phase shifts as the beam passes through the focus, so that after the focus, the wave is out of phase, i.e., has experienced a phase shift of π, with respect to a plane wave.

The entire Gouy phase evolution obtained by the windowed fitting procedure is shown in Fig. 9(a) (red line). Again, the Gouy phase term $n \cdot \arctan z/z_0$ is plotted in this case for $n = 1$ and $z_0 = 622$ μm for comparison (gray dashed line).

Similarly, for the transverse field component, the phase transition becomes steeper with increasing frequencies due to the decrease of the Rayleigh length [Fig. 9(b)]. Note that the phase curves tend to exceed the expected phase shift range of π in particular at higher frequencies, for which the field amplitudes are low and the distance strongly exceeds the Rayleigh distance. This is due to the fact that for determining the exact electric field distribution beyond the paraxial approximation, higher orders of Hermite–Gaussian functions have to be taken into account [55]. Therefore, our field projection procedure based on the assumption of circular wavefronts is strictly valid only close to the focus, leading to slight deviations beyond the Rayleigh range.

6. DISCUSSION

In Fig. 10, we schematically illustrate the phase behavior of the field components of a radially polarized beam with the 2π Gouy phase shift of the transverse and the π Gouy phase shift of the longitudinal component. At the point of highest symmetry, i.e., in the focus, the two components feature a phase difference

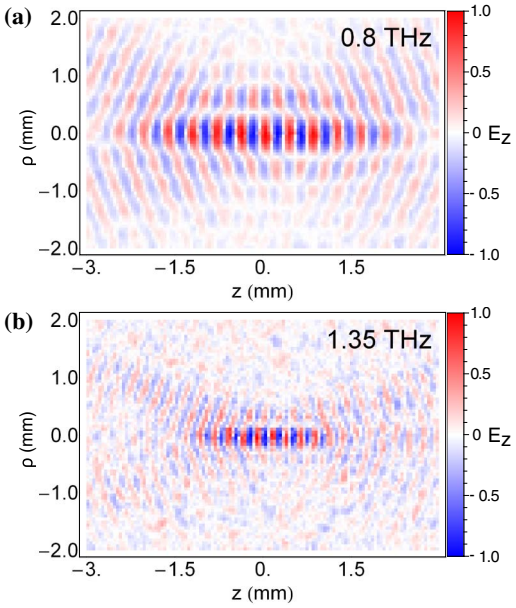

Fig. 7. Field maps in the frequency domain of the longitudinal component of the radially polarized beam at (a) 0.8 THz and (b) 1.35 THz.

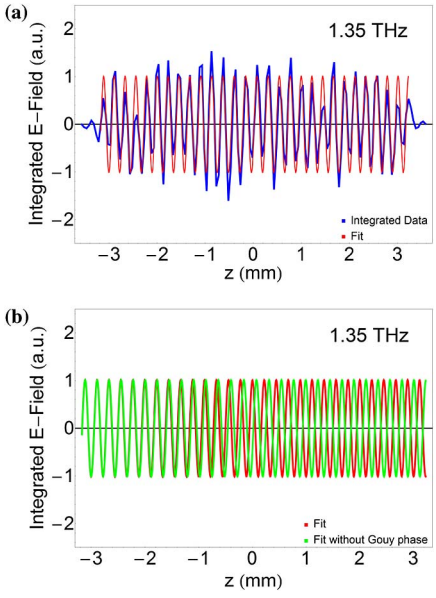

Fig. 8. Longitudinal component of the radially polarized beam: (a) projected and integrated field data and fit and (b) comparison of fit with and without Gouy phase term.

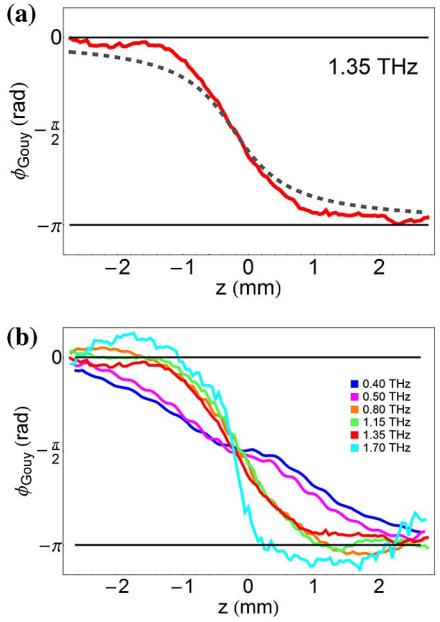

Fig. 9. Longitudinal component of the radially polarized beam: (a) Gouy phase shift at 1.35 THz and (b) compilation of several other frequencies.

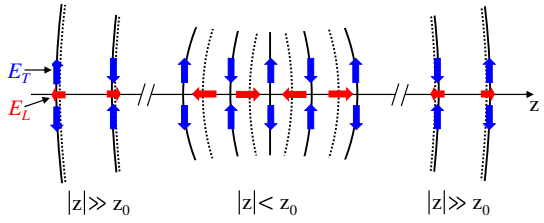

Fig. 10. Illustration of the phase shift of the transverse and longitudinal electric field components of a radially polarized beam.

of $\pi/2$ [56]. Far outside the Rayleigh range, the wavefronts for the longitudinal and transverse fields coincide; however, the direction of the longitudinal field with respect to the transverse field is opposite before and after the focus. Therefore, without having to fully map out the wavefronts, but by just taking an x–y image at a certain z-position, one can directly tell from the phase relation between the transverse and longitudinal fields whether this z-position is in front, behind, or exactly in the focal plane. This method may prove similarly useful for radially polarized terahertz beams, like the well-known knife-edge method for visible linearly polarized beams. In more quantitative terms, one can calculate the full propagating beam when only the transverse and longitudinal components are measured in the x–y plane for a *fixed value of z*.

7. CONCLUSION

In summary, we have used terahertz microscopic imaging to measure the field maps of a radially polarized beam propagating through a focus, and were able to experimentally extract the characteristic Gouy phase shift for its transverse and longitudinal electric field components for the first time. For this purpose, we have developed a procedure that allows us to extract the spatial evolution of the geometric phase of a terahertz field upon propagation through a focus. As theoretically predicted, for the radially polarized light, we observe a Gouy phase shift of 2π for the transverse and of π for the longitudinal field components. The knowledge of the Gouy phase shift, in particular of longitudinal field components of radially polarized beams, is highly relevant for a broad range of applications, ranging from particle acceleration to microscopy techniques.

Our approach, which relies on the polarization-sensitive and coherent detection of electromagnetic transients, is universal and may be used to characterize the geometric phase of focused or diffracted waves covering a wide range of the electromagnetic spectrum from microwaves up to the near infrared [57,58].

Funding. German Research Foundation (DFG) (WA 2641/7).

Acknowledgment. M.W. and K.J.K. acknowledge financial support by the German Research Foundation (DFG) through grant WA 2641/7.

See Supplement 1 for supporting content.

REFERENCES

1. L. G. Gouy, "Sur une propriété nouvelle des ondes lumineuses," C. R. Acad. Sci. **110**, 1251 (1890).
2. R. W. Boyd, "Intuitive explanation of the phase anomaly of focused light beams," J. Opt. Soc. Am. **70**, 877–880 (1980).
3. P. Hariharan and P. A. Robinson, "The Gouy phase shift as a geometrical quantum effect," J. Mod. Opt. **43**, 219–221 (1996).
4. S. Feng and H. G. Winful, "Physical origin of the Gouy phase shift," Opt. Lett. **26**, 485–487 (2001).
5. M. V. Berry, "Quantal phase factors accompanying adiabatic changes," Proc. R. Soc. A **392**, 45–57 (1984).
6. D. Subbarao, "Topological phase in gaussian beam optics," Opt. Lett. **20**, 2162–2164 (1995).
7. R. Simon and N. Mukunda, "Bargmann invariant and the geometry of the Guoy effect," Phys. Rev. Lett. **70**, 880–883 (1993).
8. A. E. Siegmann, *Lasers* (University Science Books, 1986).
9. F. Lindner, G. G. Paulus, H. Walther, A. Baltuška, E. Goulielmakis, M. Lezius, and F. Krausz, "Gouy phase shift for few-cycle laser pulses," Phys. Rev. Lett. **92**, 113001 (2004).
10. T. Tritschler, K. D. Hof, M. W. Klein, and M. Wegener, "Variation of the carrier-envelope phase of few-cycle laser pulses owing to the Gouy phase: a solid-state-based measurement," Opt. Lett. **30**, 753–755 (2005).
11. J. Arlt and M. J. Padgett, "Generation of a beam with a dark focus surrounded by regions of higher intensity: the optical bottle beam," Opt. Lett. **25**, 191–193 (2000).
12. S. M. Baumann, D. M. Kalb, L. H. MacMillan, and E. J. Galvez, "Propagation dynamics of optical vortices due to Gouy phase," Opt. Express **17**, 9818–9827 (2009).
13. A. Whiting, A. Abouraddy, B. Saleh, M. Teich, and J. Fourkas, "Polarization-assisted transverse and axial optical superresolution," Opt. Express **11**, 1714–1723 (2003).
14. M. Yi, K. Lee, J.-D. Song, and J. Ahn, "Terahertz phase microscopy in the sub-wavelength regime," Appl. Phys. Lett. **100**, 161110 (2012).
15. I. da Paz, M. Nemes, S. Padua, C. Monken, and J. P. de Faria, "Indirect evidence for the Gouy phase for matter waves," Phys. Lett. A **374**, 1660–1662 (2010).
16. T. C. Petersen, D. M. Paganin, M. Weyland, T. P. Simula, S. A. Eastwood, and M. J. Morgan, "Measurement of the Gouy phase anomaly for electron waves," Phys. Rev. A **88**, 043803 (2013).
17. W. Zhu, A. Agrawal, and A. Nahata, "Direct measurement of the Gouy phase shift for surface plasmon-polaritons," Opt. Express **15**, 9995–10001 (2007).

18. T. Feurer, N. S. Stoyanov, D. W. Ward, and K. A. Nelson, "Direct visualization of the Gouy phase by focusing phonon polaritons," Phys. Rev. Lett. **88**, 257402 (2002).
19. N. C. R. Holme, B. C. Daly, M. T. Myaing, and T. B. Norris, "Gouy phase shift of single-cycle picosecond acoustic pulses," Appl. Phys. Lett. **83**, 392–394 (2003).
20. A. A. Kolomenskii, S. N. Jerebtsov, and H. A. Schuessler, "Focal transformation and the Gouy phase shift of converging one-cycle surface acoustic waves excited by femtosecond laser pulses," Opt. Lett. **30**, 2019–2021 (2005).
21. H. Kandpal, S. Raman, and R. Mehrotra, "Observation of Gouy phase anomaly with an interferometer," Opt. Lasers Eng. **45**, 249–251 (2007).
22. Z. Wang, Z. Zeng, R. Li, and Z. Xu, "Measurement of Gouy phase shift by use of supercontinuum spectral interference," Chin. Opt. Lett. **5**, S183–S185 (2007).
23. J. H. Chow, G. de Vine, M. B. Gray, and D. E. McClelland, "Measurement of Gouy phase evolution by use of spatial mode interference," Opt. Lett. **29**, 2339–2341 (2004).
24. P. Bon, B. Rolly, N. Bonod, J. Wenger, B. Stout, S. Monneret, and H. Rigneault, "Imaging the Gouy phase shift in photonic jets with a wavefront sensor," Opt. Lett. **37**, 3531–3533 (2012).
25. S. Hunsche, S. Feng, H. G. Winful, A. Leitenstorfer, M. C. Nuss, and E. P. Ippen, "Spatiotemporal focusing of single-cycle light pulses," J. Opt. Soc. Am. A **16**, 2025–2028 (1999).
26. A. B. Ruffin, J. V. Rudd, J. F. Whitaker, S. Feng, and H. G. Winful, "Direct observation of the Gouy phase shift with single-cycle terahertz pulses," Phys. Rev. Lett. **83**, 3410–3413 (1999).
27. R. W. McGowan, R. A. Cheville, and D. Grischkowsky, "Direct observation of the Gouy phase shift in THz impulse ranging," Appl. Phys. Lett. **76**, 670–672 (2000).
28. X. Wang, W. Sun, Y. Cui, J. Ye, S. Feng, and Y. Zhang, "Complete presentation of the Gouy phase shift with the THz digital holography," Opt. Express **21**, 2337–2346 (2013).
29. D. G. Hall, "Vector-beam solutions of Maxwell's wave equation," Opt. Lett. **21**, 9–11 (1996).
30. Q. Zhan, "Cylindrical vector beams: from mathematical concepts to applications," Adv. Opt. Photon. **1**, 1–57 (2009).
31. S. Quabis, R. Dorn, M. Eberler, O. Glöckl, and G. Leuchs, "Focusing light to a tighter spot," Opt. Commun. **179**, 1–7 (2000).
32. H. P. Urbach and S. F. Pereira, "Field in focus with a maximum longitudinal electric component," Phys. Rev. Lett. **100**, 123904 (2008).
33. H. Wang, L. Shi, B. Lukyanchuk, C. Sheppard, and C. T. Chong, "Creation of a needle of longitudinally polarized light in vacuum using binary optics," Nat. Photonics **2**, 501–505 (2008).
34. S. W. Hell and J. Wichmann, "Breaking the diffraction resolution limit by stimulated emission: stimulated-emission-depletion fluorescence microscopy," Opt. Lett. **19**, 780–782 (1994).
35. T. D. Visser and J. T. Foley, "On the wavefront spacing of focused, radially polarized beams," J. Opt. Soc. Am. A **22**, 2527–2531 (2005).
36. H. Chen, Q. Zhan, Y. Zhang, and Y.-P. Li, "The Gouy phase shift of the highly focused radially polarized beam," Phys. Lett. A **371**, 259–261 (2007).
37. X. Pang and T. D. Visser, "Manifestation of the Gouy phase in strongly focused, radially polarized beams," Opt. Express **21**, 8331–8341 (2013).
38. E. A. Nanni, W. R. Huang, K.-H. Hong, K. Ravi, A. Fallahi, G. Moriena, R. J. Dwayne Miller, and F. X. Kartner, "Terahertz-driven linear electron acceleration," Nat. Commun. **6**, 8486 (2015).
39. R. Dorn, S. Quabis, and G. Leuchs, "Sharper focus for a radially polarized light beam," Phys. Rev. Lett. **91**, 233901 (2003).
40. G. Miyaji, N. Miyanaga, K. Tsubakimoto, K. Sueda, and K. Ohbayashi, "Intense longitudinal electric fields generated from transverse electromagnetic waves," Appl. Phys. Lett. **84**, 3855–3857 (2004).
41. B. Hao and J. Leger, "Experimental measurement of longitudinal component in the vicinity of focused radially polarized beam," Opt. Express **15**, 3550–3556 (2007).
42. G. Chang, C. J. Divin, C.-H. Liu, S. L. Williamson, A. Galvanauskas, and T. B. Norris, "Generation of radially polarized terahertz pulses via velocity-mismatched optical rectification," Opt. Lett. **32**, 433–435 (2007).
43. J. Deibel, M. Escarra, and D. Mittleman, "Photoconductive terahertz antenna with radial symmetry," Electron. Lett. **41**, 226–228 (2005).
44. J. Deibel, M. Escarra, N. Berndsen, K. Wang, and D. Mittleman, "Finite-element method simulations of guided wave phenomena at terahertz frequencies," Proc. IEEE **95**, 1624–1640 (2007).
45. T.-I. Jeon, J. Zhang, and D. Grischkowsky, "THz Sommerfeld wave propagation on a single metal wire," Appl. Phys. Lett. **86**, 161904 (2005).
46. S. Waselikowski, C. Fischer, J. Wallauer, and M. Walther, "Optimal plasmonic focusing on a metal disc under radially polarized terahertz illumination," New J. Phys. **15**, 075005 (2013).
47. S. Winnerl, B. Zimmermann, F. Peter, H. Schneider, and M. Helm, "Terahertz Bessel-Gauss beams of radial and azimuthal polarization from microstructured photoconductive antennas," Opt. Express **17**, 1571–1576 (2009).
48. A. Bitzer, A. Ortner, and M. Walther, "Terahertz near-field microscopy with subwavelength spatial resolution based on photoconductive antennas," Appl. Opt. **49**, E1–E6 (2010).
49. A. Adam, "Review of near-field terahertz measurement methods and their applications," J. Infrared, Millimeter, Terahertz Waves **32**, 976–1019 (2011).
50. A. Bitzer, H. Merbold, A. Thoman, T. Feurer, H. Helm, and M. Walther, "Terahertz near-field imaging of electric and magnetic resonances of a planar metamaterial," Opt. Express **17**, 3826–3834 (2009).
51. M. Walther and A. Bitzer, "Electromagnetic wave propagation close to microstructures studied by time and phase-resolved THz near-field imaging," J. Infrared, Millimeter, Terahertz Waves **32**, 1020–1030 (2011).
52. M. A. Seo, A. J. L. Adam, J. H. Kang, J. W. Lee, S. C. Jeoung, Q. H. Park, P. C. M. Planken, and D. S. Kim, "Fourier-transform terahertz near-field imaging of one-dimensional slit arrays: mapping of electric-field-, magnetic-field-, and Poynting vectors," Opt. Express **15**, 11781–11789 (2007).
53. J. R. Knab, A. J. L. Adam, M. Nagel, E. Shaner, M. A. Seo, D. S. Kim, and P. C. M. Planken, "Terahertz near-field vectorial imaging of subwavelength apertures and aperture arrays," Opt. Express **17**, 15072–15086 (2009).
54. A. Bitzer, A. Ortner, H. Merbold, T. Feurer, and M. Walther, "Terahertz near-field microscopy of complementary planar metamaterials: Babinet's principle," Opt. Express **19**, 2537–2545 (2011).
55. H.-C. Kim and Y. H. Lee, "Hermite-Gaussian and Laguerre-Gaussian beams beyond the paraxial approximation," Opt. Commun. **169**, 9–16 (1999).
56. S. Winnerl, R. Hubrich, M. Mittendorff, H. Schneider, and M. Helm, "Universal phase relation between longitudinal and transverse fields observed in focused terahertz beams," New J. Phys. **14**, 103049 (2012).
57. C. Kübler, R. Huber, S. Tübel, and A. Leitenstorfer, "Ultrabroadband detection of multi-terahertz field transients with GaSe electro-optic sensors: approaching the near infrared," Appl. Phys. Lett. **85**, 3360–3362 (2004).
58. M. Eisele, T. L. Cocker, M. A. Huber, M. Plankl, L. Viti, D. Ercolani, L. Sorba, M. S. Vitiello, and R. Huber, "Ultrafast multi-terahertz nano-spectroscopy with sub-cycle temporal resolution," Nat. Photonics **8**, 841–845 (2014).